Optofluidic microcavities: Dye-lasers and biosensors

Y. Chen,[1,2,3,a)] L. Lei,[1,2] K. Zhang,[1] J. Shi,[2] L. Wang,[2] H. Li,[2,3] X. M. Zhang,[1] Y. Wang,[1] and H. L. W. Chan[1]
[1]*Department of Applied Physics, The Hong Kong Polytechnic University, Hong Kong, China*
[2]*Ecole Normale Supérieure, CNRS-ENS-UPMC, 24 rue Lhomond, 75231 Paris, France*
[3]*Centre for Microfluidics and Nanotechnology, Peking University, 100871 Beijing, China*

(Received 5 August 2010; accepted 22 September 2010; published online 30 December 2010)

Optofluidic microcavities are integrated elements of microfluidics that can be explored for a large variety of applications. In this review, we first introduce the physics basis of optical microcavities and microflow control. Then, we describe four types of optofluidic dye lasers developed so far based on both simple and advanced device fabrication technologies. To illustrate the application potential of such devices, we present two types of laser intracavity measurements for chemical solution and single cell analyses. In addition, the possibility of single molecule detection is discussed. All these recent achievements demonstrated the great importance of the topics in biology and several other disciplines. © *2010 American Institute of Physics.* [doi:10.1063/1.3499949]

I. INTRODUCTION

Light standing waves can be formed in an optical cavity at certain frequencies due to specular multireflections. Because of the light confinement, the interaction of light with matters inside the cavity can be much enhanced and the resonant cavity modes can be extremely sharp. These two properties have led to the invention of lasers and high accuracy instruments such as interferometers. At microscales, optical cavities can be easily produced and integrated in various microsystems. If the fabrication quality is sufficiently high, the cavity systems can be explored in the study of quantum electrodynamics as well as advanced optoelectronic devices.[1,2]

Optofluidic microcavities can be designed based on physics of optics and microfluidics,[3,4] taking into account the availability of micro- and nanofabrication technologies.[5] Similar to the more conventional systems, optofluidic microcavities are used for light manipulation. Of particular interest is to produce dye laser sources on a chip for several reasons. First, different types of organic dye molecules are available, which cover a broad range of laser emission wavelengths.[6] Second, by changing the dye types and/or dye concentration with microfluidics, the laser emission wavelength can be tuned with high precision. Indeed, microfluidic devices allow manipulating solutions with high spatial and temporal resolution.[7] The integration of optical cavities into microfluidic devices provides unique combination to address the high sensitivity detection problems. For example, they could be used for laser intracavity absorption measurements of very small volume and low concentration samples.[8] Finally, the dimension of optofluidic microcavities can be sufficiently small and integrated for the mass fabrication of compact and portable devices. Therefore, they hold high potential in applications for biosensing and high throughput screening, which are generally required in biomedical research, drug discovery, and clinical diagnosis.

The concept of optofluidics has been founded less than 10 years ago. In 2003, Kristensen *et*

a)Author to whom correspondence should be addressed. Ecole Normale Supérieure, 24 rue Lhomond, 75005 Paris, France. Electronic mail: yong.chen@ens.fr.

al.[9] proposed the first optofluidic dye laser based on the general concept of microfluidics. To obtain a Fabry–Pérot cavity, they fabricated two gold coated surfaces, one placed on the top and another on the bottom of a 10 μm deep and 1 mm wide microfluidic channel. When a dye solution (Rhodamine-6G in ethanol) was injected in and pumped with a pulsed Nd:yttrium aluminum garnet (YAG) laser at 532 nm, a laser emission at 570 nm could be observed. By using the simple soft lithography processes,[10] Chen *et al.*[11–13] fabricated a variety of optofluidic elements such as lenses, prisms, couplers, and beam splitters. They also demonstrated the liquid core waveguides with integrated optical fibers for efficient light coupling and spectroscopic analyses of reactive biomolecules. By using the property of laminar flow in microfluidics, Whitesides *et al.*[14] created high quality liquid core waveguides by using two liquids of different refractive indices. Finally, in Summer 2004, a collaborative project has been launched in the USA as a milestone of optofluidics.[15] Afterward, many optofluidic devices could be studied for the purposes of either micro-optic engineering or bioapplications. The early research activities were then reviewed by Psaltis *et al.* in 2006 (Ref. 16) and Monat *et al.* in 2007.[17] More systematic description of the topics can now be found in a recent book edited by Fainman *et al.*[18]

In this review, we focus on optofluidic dye lasers and some potential applications of optofluidic microcavities in chemistry and biology. Based on our own research works and previous presentations,[15–19] we try to provide a more consistent description of the subject with an enlarged view on the historical development as well as cross-disciplinary perspectives. The paper is organized as follows. First, we introduce in Sec. II physics essentials of optofluidic microcavities. In Sec. III, we review different types of optofluidic dye lasers. Then, we present in Sec. IV a few of typical applications in optofluidics. Finally, we discuss some future directions in Sec. V.

II. PHYSICS OF OPTOFLUIDIC MICROCAVITIES

The physics of optofluidic microcavities relies on both physics of optical cavities and that of microflow control. The physics of optical cavities as well as their advanced applications can be found in many text books.[1,2,20,21] The physics of microflow control is essentially the same of that in fluid mechanics under small Reynolds number conditions.[3,4] In such a case, the laminar flow is dominant, and the calculation of flow velocity is relatively simple. However, because of the much increased surface-to-volume ratio, surface effects become important. Considerable efforts were also devoted to investigations such as droplet generation, hydrodynamic focusing, wetting, electrowetting, and electro-osmotic and electrokinetic pumping as well as transportation through nanopores and nanochannels. All these effects critically depend on the surface properties of the construction or coating materials of micro and nanofluidic channels.

A. Physics of optical or optofluidic microcavities

Optical microcavities can be made or operated with or without using fluids. When an optical microcavity is partially or fully filled of a fluid, it can be considered as an optofluidic element or optofluidic microcavity. Alternatively, an optical microcavity submerged in a microflow can also be considered an optofluidic system because of the possibility of dynamically manipulating the surrounding medium of the cavity. Accordingly, optofluidic microcavities can be classified broadly into two categories: *cavity containing fluid* and *cavity in fluid.*

The form of the cavity can be very different, ranging from thin layer slabs, liquid droplets, and solid microspheres to more laboriously engineered microrings, microdisks, and microtoroids.[1,2] The mirrors of the cavity can be made of liquid-air, liquid-solid, or solid-air interfaces as well as high reflection metallic layers, dielectric multilayers, or periodic three-dimensional structures. In particular, Bragg gratings and photonic band structures are now widely used for light confinements and accurate manipulation of optical waves. Without going into much detail, we review some simple formulations by considering two types of cavity structures: one relying on back-and-forward multireflection and the other relying on recycling total internal reflection.

In the case of back-and-forward multireflection in a slab cavity (Fabry–Pérot etalon), standing waves can be formed for the wavelengths defined by

$$m\lambda = 2nL, \quad m = 1,2,3 \ldots , \tag{1}$$

where λ is the wavelength, L is the cavity length, and n the refractive index of the cavity medium. The free spectra range (FSR) is defined by the wavelength difference between two neighbor modes, i.e.,

$$\Delta\lambda_{\mathrm{FSR}} = \lambda^2/2nL. \tag{2}$$

The transmission spectrum of the slab cavity can be calculated analytically or numerically by using the matrix transfer method.[20] Then, the finesse ($F=\Delta\lambda_{\mathrm{FSR}}/\delta\lambda$) and the quality factor (Q) of the cavity can be deduced, $\delta\lambda$ being defined as the full width at half maximum (FWHM) of the transition peaks, which depends on the quality of reflecting mirrors and the quality of the etalon. For *Lorentzian* peaks, $Q=\lambda/\delta\lambda$.

For a cavity of $n=1.5$ and $L=0.2$ μm, the first order cavity mode occurs at $\lambda=0.6$ μm with $\Delta\lambda_{\mathrm{FSR}}=0.6$ μm. If $Q=10^2$, $\delta\lambda=6$ *nm*. Using the same parameters except $L=20$ μm, we obtain $\Delta\lambda_{\mathrm{FSR}}=6$ nm, which is still in the limit the spectral resolution of the cavity.

A ring cavity can be formed with more than two mirrors in which light propagation is unidirectional. In particular, the total internal reflection in a spherical cavity leads to the so-called Whispering Gallery modes, defined by

$$m\lambda \approx 2\pi nR, \quad m = 1,2,3 \ldots , \tag{3}$$

$$\Delta\lambda_{\mathrm{FSR}} = \lambda^2/2n\pi R, \tag{4}$$

where R is the radius of the sphere. Similarly, other cavity parameters can be defined or calculated.

Bragg gratings are made of periodic dielectric layers with a quarter λ effective thickness for each layer. The center wavelength of its high reflection or stop band is defined by

$$m\lambda/2 = n_1L_1 + n_2L_2, \quad m = 1,2,3 \ldots , \tag{5}$$

where $n_1(n_2)$ and $L_1(L_2)$ are, respectively, the refractive index and thickness of layer 1(2). The reflection power and the stop bandwidth of Bragg mirrors increase with the total number and the refractive index contrast of the two types of dielectric layers. A numerical calculation of Bragg refection can be easily performed by using again the matrix transfer method.[20]

In the case of Fabry–Pérot etalon, the energy output can be controlled by regulating the reflection power of one of the mirrors or by other means. For ring cavities, the energy output can be regulated by evanescent wave coupling of the ring with a waveguide. The coupling efficiency between the ring cavity and the waveguide can be calculated using the matrix transfer method described in Ref. 22. More generally, the cavity modes of all coupled systems including photonic crystals can be numerically determined based on Maxwell equations.[20–22]

The electronic states of the cavity medium can be uniformly or partially active or excitable. Under resonance conditions, light-matter interaction can be strongly enhanced so that quantum electrodynamic effects become observable including laser emission, Rabi splitting, quantum entanglement, polariton condensation, etc. The coupling efficiency between a cavity mode and an electron state can be calculated based on Maxwell equations taking into account the contribution and the specificity of the resonant electron states.[23–28]

B. Physics of microflow control

In fluid mechanics, the Navier–Stokes equation is used to determinate the fluidic motions,[3,4]

$$\rho\left[\left(\frac{\partial v}{\partial t} + v \,.\, \nabla\right)v\right] = f_{\mathrm{ext}} - \nabla p + \eta\Delta v, \tag{6}$$

where ρ and η are, respectively, the density and the viscosity of the liquid, v is the velocity, p is the pressure, and f_{ext} the contribution of applied forces.

Let us first consider a pressure driven liquid motion. In the absence of external forces ($f_{\text{ext}}=0$) and under the condition of small Reynolds number ($\text{Re}=|\rho(v\cdot\nabla)v|/|\eta\Delta v|\approx\rho UL/\eta$) and noncompressive liquid ($\nabla\cdot v=0$), U and L being typical velocity and length scales, the Navier–Stokes equation becomes

$$\eta\Delta v=\nabla p. \tag{7}$$

For a cylindrical channel of inner diameter R and length l, which is filled of a fluid subjected to a pressure difference Δp between the two ends, Eq. (7) can be solved with the boundary condition $v(R)=0$, giving a parabolic speed distribution (Poiseuille law),

$$v(r)=\frac{\Delta p}{4\eta l}(R^2-r^2), \tag{8}$$

where r is the distance to the center of the channel. From Eq. (8), one can also calculate the average velocity and the flow rate for a given set of parameters.

Alternatively, the liquid motion can be driven by applying an electric field along the channel. The motion is then called electro-osmotic, which can be understood as follows. At the interface, the interaction between the charges in solid and those in liquid results in a charged double layer at the surface of the microchannel wall, one fixed and another mobile under applied electric field. Because of the viscosity of the liquid, this motion is global and proportional to the electric field strength, i.e.,

$$V_{\text{eo}}=\mu_{\text{eo}}E, \tag{9}$$

where $\mu_{\text{eo}}=\lambda_D\sigma_0/\eta$ is called the electro-osmotic mobility, σ_0 being the surface charge density and $\lambda_D=(\varepsilon_w k_B T/2n_0e^2)^{1/2}$ being the Debye length of the double layer, which can be calculated using the Poisson's equation,

$$\Delta\psi=-\rho/\varepsilon_w, \tag{10}$$

where $\rho=e(n_+-n_+)$ and $n_\pm=n_0\exp(\mp e\psi/k_BT)$, ε_w being the permittivity of the solution, k_B being the Boltzmann constant, and T being the temperature. Unlike the pressure driven flow, the electro-osmotic flow is much more homogeneous in speed distribution, with the exception in the region closed to the wall.

Both pressure and electro-osmotic forces are frequently used to control the motion of microflows. However, some other methods such as capillary and electrocapillary forces, electrowetting, electrokinetic pumping, piezoelectric or acoustic pumping, thermogradient, etc. can all be used for microflow motion control in optofluidic experiments.

III. OPTOFLUIDIC DYE LASERS

So far, most of the investigations on optofluidic dye lasers were developed with Rhodamine 6G dye molecules in ethanol as gain medium flowing in microfluidic cavities. When pumped above threshold with Nd:YAG laser pulses (532 nm, 0.5 ns, 5 kHz), dye laser emission around 570 nm can be observed. To avoid photobleaching, the dye solution has to be circulated at a typical flow rate of 5 mm/s.

The electron states of Rhodamine 6G in the frequency region of interest can be schematically represented by three energy bands: S_0, S_1, (singlet ground and first excited states) and T_1 (triplet first excited states).[6] Pumping electrons from S_0 to S_1 leads to a high population of T_1 band because of the fast relaxation (nanosecond) from S_1 to T_1, whereas T_1 states are metastable but with a much longer decay time (millisecond) from T_1 to S_0, unless stimulated. Above the laser threshold, the high population in T_1 is maintained and the gain is larger than the loss of the whole system so that light amplification stimulated emitting radiation (laser) occurs.

Experimentally, optofluidic dye lasers can be made for in-plane or out-plane emission. Although the out-plane configuration demonstrated by Kristensen *et al.*[9] can be used for some

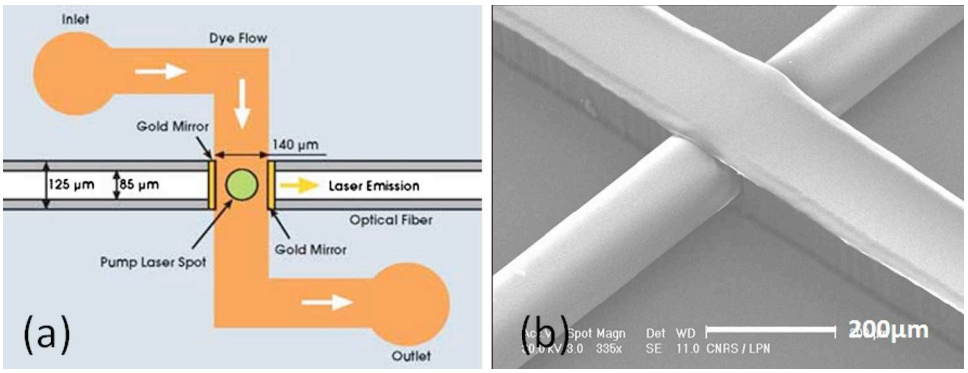

FIG. 1. (a) Schematic of an optofluidic microcavity with a microfluidic channel (yellow) passing through the cavity between two optical fibers with gold coated end-facets (Ref. 30) and (b) SEM image of a mold obtained by photolithography with an embedded optical fiber (Ref. 32).

applications, it is obvious that the in-plane configuration has more advantages in term of device integration. Moreover, soft lithography[10] allows easy monolithic processing with polydimethylsiloxane (PDMS). To begin with, Chen *et al.* proposed a laser cavity simply formed with two end-facet gold coated optical fibers.[29–33] Such a device configuration allows not only an efficient light coupling but also an easy microfluidic manipulation. Vezenov *et al.* reported an optofluidic dye laser based on liquid-liquid waveguide and a long optical cavity.[34] By using soft lithography techniques, Balslev and Kristensen[35] realized 130th Bragg grating for mirror reflection. Then, Li *et al.* succeeded in single mode operation by using 15th and then fifth order distributed feedback structure.[36,37] Lower order Bragg gratings were fabricated by soft UV nanoimprint[38] and thermal nanoimprint[39,40] lithography techniques. In addition, Gerborg–Hansen and Kristensen[41] and Song *et al.*,[42] respectively, used more conventional lithography techniques (electron beam lithography and optical lithography) to demonstrate dye lasers with evanescent wave coupling with regular or circular Bragg mirrors. Note that the high resolution patterning achieved by Peroz *et al.*[38] and Vannahme *et al.*[39,40] is a low cost and high throughput technique, which can be applied to industrial manufacturing and the fabrication of many other types of nanophotonic structures, including Bragg gratings, photonic crystals, and nanoplasmonic patterns.[43–45] This technique is also compatible to more conventional patterning techniques, allowing easy fabrication of multilevel devices with fine alignment.[46–49] Alternatively, nanoembossing techniques can be used for production of all plastic devices.[50]

A. Optical fiber based microcavity

Light coupling into microfluidic devices is challenging because of the requirement of high coupling efficiency, high mechanic stability, and high signal-to-noise ratio. One solution is integrating optical fibers directly into microfluidic channels. By using two aligned optical fibers of 125 μm diameter with a separation distance of 100 μm perpendicular to a channel of dye solution, many applications could be developed[11–13,29–34,51,52] [Fig. 1(a)].

The microcavity mirrors can be obtained by depositing 20 nm Ti and 100–300 nm Au film directly on the end of the two cleaved fibers. Then, they can be integrated into a microfluidic device fabricated by soft lithography. In order to obtain a better insertion of the two optical fibers, a fiber was embedded in the SU8 resist mold [Fig. 1(b)], which could be fabricated by first fixing the fiber on a silicon substrate (with two adhesive types) and then processing the conventional photolithography with SU8 resist. After casting, curing, and separation of PDMS layer, the two metalized fibers were inserted, and connection holes were punches before thermal bonding on a glass substrate. With a dye solution of Rhodamine 6G pumped at 532 nm, optical cavity modes and laser emission could be observed below and above laser threshold (Fig. 2). Changing the type of dye molecules leads to the change of the laser emission wavelength. By using a mixture of two

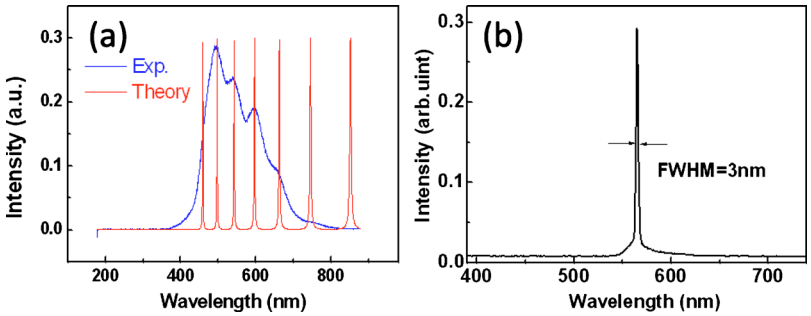

FIG. 2. (a) Photoluminescence of Rhodamine 6G confined in a microcavity and calculated cavity modes (Ref. 12) and (b) emission spectrum of a typical optofluidic dye laser pumped above laser threshold (Ref. 33).

types of dye molecules, i.e., Rhodamine 6G and surforhodamine 101, in ethanol, collinear dual-color (yellow and red) laser emission could be obtained, showing a clear correlation of the laser intensity of the two peaks.

B. Bragg grating based microcavity

Distributed feedback (DFB) dye lasers use Bragg gratings for single mode operation. By using conventional soft lithography, high order Bragg mirrors could be produced.[34–36] Figure 3 shows a phase shifted 15th order DFB structure (period of 3 μm and length of 8 mm) coupled to a liquid core wave guide of single transverse mode.[37] When pumped with 6 ns, 532 nm laser pulses, laser emission with a linewidth of 0.21 nm was observed above a threshold of 0.8 $\mathrm{mJ/cm^2}$.

To decrease the size and the scattering loss of the device, lower order optofluidic DFB dye lasers were fabricated by soft UV or thermal nanoimprint lithography[38–40] or more conventional lithography techniques.[41] As mentioned above, soft UV and thermal nanoimprint lithography has a clear advantage of low cost and high throughput. In soft UV nanoimprint lithography, a PDMS stamp was replicated from a master defined by electron beam lithography and reactive ion etching techniques. Then, it was used for imprinting a photo curable resist spin coated on a substrate. After UV exposure, the imprinted structure was transferred into the substrate by lift-off and reactive ion etching. With a bilayer resist process, high aspect ratio and low order Bragg gratings could be produced on glass substrates. Afterward, a PDMS layer with microfluidic channels was aligned and bonded on Bragg grating substrate. Figure 4(a) shows a 400 nm half pitch Bragg grating (third order) etched into a fused silica ($n=1.46$) with an etch depth of 2.8 μm. According to the Schur recursive algorithm,[53] the third resonant wavelength should be 535 nm with a bandwidth of about 40 nm. Taking into account the emission properties of Rhodamine 6G in the range of 500–650 nm, a laser emission at wavelength 555 nm could be expected. Two third Bragg gratings were patterned with a separation of 100 μm, one covering an area of 250×250 $\mu\mathrm{m}^2$ (higher reflector)

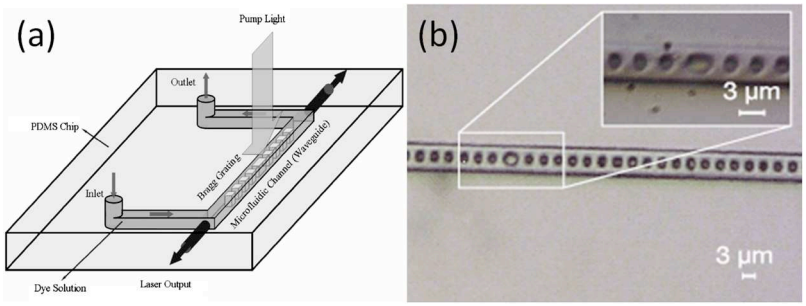

FIG. 3. (a) Schematic of optofluidic dye laser for single mode operation and (b) SEM image of a 15th order Bragg grating with a phase shifter obtained by soft lithography (Ref. 36).

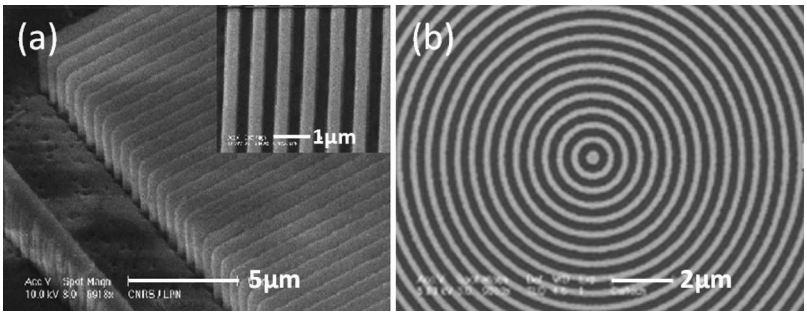

FIG. 4. (a) SEM pictures of a third order Bragg grating for a distributed feedback dye laser operating at 570 nm (Ref. 38) and (b) SEM image of a circular grating for optofluidic evanescent dye laser operation (Ref. 42).

and another of 250×200 μm^2 (lower reflector). When pumped with a pulsed Nd:YAG laser (532 nm, 0.5 ns and 10 kHz), laser emission was obtained at a threshold of 12 $\mu J/mm^2$. More recently, Vannahme *et al.* fabricated the first order Bragg gratings in thin layers of cyclic olefin copolymer by thermal nanoimprint, allowing observation of laser emission peaks with Pyrromethene 597 in benzyl alcohol as dye solution.[39] These authors also used the same technique to replicate the first order Bragg gratings in polymethyl methacrylate for solid state lasers.[40]

Finally, Song *et al.*[42] demonstrated an optofluidic dye laser with an embedded circular DFB grating [Fig. 4(b)]. The dye solution above the solid DFB grating also acts as the cladding layer. With R6G dye solution, single mode operation is obtained at 571 nm with a pumping threshold of 9.5 $\mu J/pulse$. In such a configuration, the laser mode is confined within the grating, and the optical gain is due to evanescent coupling of the laser mode with the fluids so that a wide range of fluid refractive indices (even lower than PDMS) can be used for stable and narrow-linewidth laser emissions.

C. Microring cavities

Optofluidic ring lasers can also be fabricated by monolithic processes of PDMS. Different types of ring cavities were designed based on the principle of the one-way total internal reflection. Galas *et al.* patterned a microring cavity with four air-in-PDMS mirrors. By injecting a low refractive index liquid (ethanol) into one of the air chambers, dye laser emission could be coupled into a waveguide for output recording.[54] By adding a second microfluidic layer, the dye flow could be controlled with integrated valves, pumps, and mixers. The fluorescence and laser spectra were recorded as a function of pumping energy density. At a R6G concentration of 0.01 mol/L and a flow velocity of 5 mm/s, a laser threshold of 15 $\mu J/mm^2$ was demonstrated with a full linewidth at half maximum of about 6 nm [Fig. 2(b)].

Figure 5 shows a single mode liquid core microring structure of 300 μm diameter coupled

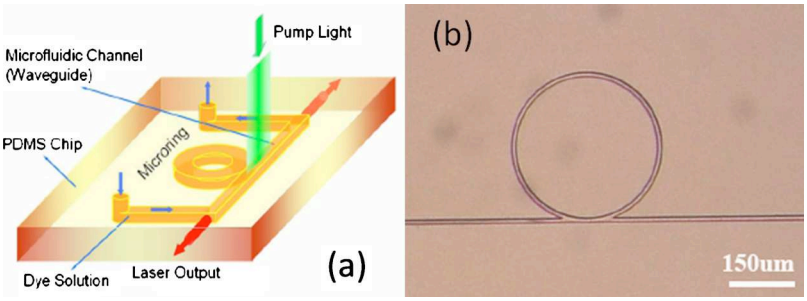

FIG. 5. (a) Schematic of an optofluidic dye laser with microring cavity and (b) microphotograph of a microring cavity coupled to a single mode waveguide in PDMS (Ref. 55).

with a waveguide of 2×3 μm^2 cross-section.[55] Such a device was obtained also by monolithic casting of PDMS. When filled with a Rhodamine 6G dye solution and pumped with a 532 nm Nd:YAG laser, a laser threshold of 9.2 nJ could be demonstrated due to small size of the ring cavity.

Alternatively, polished fiber prisms and tapered optical fibers were both used to directionally couple out the laser emission.[56] Here, the microring was obtained by drawing fused silica preform, resulting in an outer diameter of 75 μm and a wall thickness of 5 μm. The fiber prisms were fabricated by angled polishing (15°) a 200 μm multimode fiber, and the tapered fibers were obtained by pulling multimode optical fibers under intense heat to reach a minimum diameter of 3 μm. Afterward, the fiber prisms or tapered fibers were placed close to the microring and fixed by PDMS casting and curing at 70° for 2 h. As results, the system provided a Q-factor larger than 10^6 and a laser threshold less than 1 $\mu J/mm^2$. By fusing an optical fiber (125 μm) on the inner surface of a glass capillary (900 μm inner diameter) serving as a fluidic channel, the same group has shown laser oscillation with a threshold of 7 $\mu J/mm^2$ per pulse.[57]

D. Tunable dye lasers

The laser emissions can be modified by changing optofluidic microcavity parameters. For small range tuning, dynamic changing of the dye concentration should be easy with integrated micro-valves and pumps.[54] Alternatively, mechanic tuning could be possible by stretching or compressing optofluidic microcavities due to the small Young's modules of PDMS. This was demonstrated with an integrated PDMS-air gap etalon controlled by air pressure. In such a device, the dye laser microcavity is enclosed by two air chambers, one with a tilted mirror and another having two parallel PDMS/air interfaces for pneumatic tuning of the mirror reflection properties. A tuning range of 14 nm could then be achieved in the pressure range of 2–30 psi.[58]

For a larger range wavelength "tuning," it is more appropriate to use several types of dye molecules on the same chip. By using a mixture of R6G and Rhodamine 101 for example, multicolor laser emission could be obtained for a wavelength range of 60 nm.[59] The integration of multiple DFB dye lasers on the same device could also be possible to have a few emission wavelengths.[37] Alternatively, one should be able to manipulate dye solutions with integrated valves and pumps so that a large range wavelength tuning of laser emissions should be possible for sensing and spectroscopic applications.

In microfluidics, considerable efforts were devoted for the generation and manipulation of droplets in microfluidic channels. Because of the surface energy minimization, the interface between droplets and carrier fluids should be optically smooth, providing ideal cavity model for laser at whispering gallery modes if the refractive index of the droplet is higher than that of the carrier liquid. By generating a train of alternating droplets containing solutions of different dyes in a microfluidic channel, Tang *et al.* demonstrated such a dye laser with multicolors in the range between 580 and 680 nm at a switching frequency of up to 3.6 kHz (Fig. 6).[60] Such a device is believed to be useful for a variety of applications such as on-chip spectroscopy and flow cytometry.

Finally, the emission intensity of optofluidic dye lasers can also be tuned with integrated microfluidic elements. For example, by using hydrodynamic focusing technique and a dye solution as either focusing flow or focused flow, the stream bandwidth of dye flow and the laser emission intensity could be tuned dynamically with changing pressure in the three stream system.[31]

IV. BIOSENSOR APPLICATIONS

The application efforts of microfluidics have been mainly devoted to life sciences.[61–65] It is known that high sensitivity biosensing of single molecules and single cells are still challenging in terms of both tool development and application suitability. Among many interesting topics, investigations on stem cells including embryonic stem cells, induced pluripotent stem cells, and other tissues stem cells are of primary importance. Optofluidic microcavities and other microfluidic methods are certainly helpful for the improvement of our understanding on how cell processes are

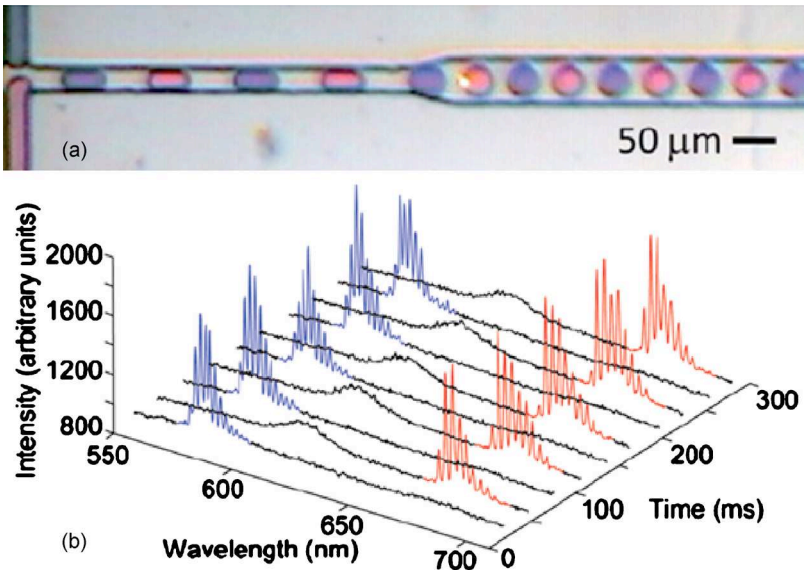

FIG. 6. (a) Microphotograph of droplet microcavities containing alternatively two types of dye solutions generated in a microfluidic channel and (b) corresponding dye laser spectra recorded in the range between 500 and 700 nm at switching frequency up to 3.6 kHz (Ref. 60).

programmed and how they can be regulated or reprogrammed. Since these problems are also related to cancer development and aging issues, the im portance of such an application should never be overestimated. In principle, each type of cells and each cell at different phase of a cell cycle should have specific optical response to electromagnetic waves. Optofluidic microcavities provide unique solutions for diagnosis because of the resonant interaction and enhanced nonlinear effects. Therefore, they can be used to largely improve the performances of cell sorting as well as high throughput screening cell assays. Similarly, they can be used for a better identification of cell factors without biomarkers and a higher detection sensitivity of DNA or protein microarrays. Up to date, however, optofluidic microcavities have not yet been successfully implemented for practical uses but the reported demonstrations clearly showed a high potential for the future applications.

A. Analyses of chemical and biochemical solutions

The laser emission is highly sensitive to changes in absorption, scattering, refractive index, or other types of perturbations inside the laser cavity. In particular, the laser output becomes extremely sensitive to the change of the gain efficiency when the excitation intensity is slightly above the pumping threshold. Then, laser intracavity detection can be applied for much increased sensitivity.[8]

Figure 7(a) shows a microphotograph of the device in which two microfluidic channels are patterned inside a cavity formed by two gold coated optical fibers. In one of the channels, a dye molecule solution is injected as liquid gain medium. In another channel, a nanoliter sample solution can be injected for high sensitivity detection. To evaluate the performance of this method, methylene blue dye dissolved in water was injected into the sample channel. Figure 7(b) displays the intensity ratio of the dye laser output (full squares) as a function of absorbent concentration at a constant pumping power (38 $\mu J/mm^2$). As expected, a much enhanced detection capability with a low concentration down to 10^{-6} mol/l could be demonstrated.

In Fig. 7(b), the results of the numerical calculation are also plotted for both laser intracavity absorption (dashed line) and conventional single pass absorption (solid line). The Beer–Lambert law was used to calculate the single pass absorption, i.e.,

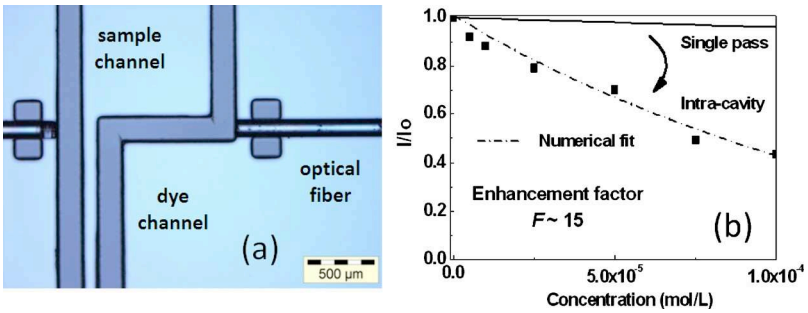

FIG. 7. (a) Microphotograph of an optofluidic device used for laser intracavity absorption measurements and (b) measured laser output intensity as a function of absorbent concentrations (full squares). The results of numerical calculations are also plotted for single pass (dotted line) and intracavity (dashed line) modeling (Ref. 8).

$$I = I_0 \exp(-\alpha L_a C), \tag{11}$$

where I_0 and I are, respectively, the light intensity before and after passing the sample solution, L_a is the optical path length, and α and C are, respectively, the absorption coefficient and the concentration of the absorbent molecules. The solid line was obtained with $\alpha \approx 28\,000\ 1\,\mathrm{M}^{-1}\,\mathrm{cm}^{-1}$ and $L_a = 150\ \mu\mathrm{m}$.

The same parameters were used for laser intracavity absorption, taking into account the gain and the absorbent of the system. The gain of the system can be expressed by

$$G = gL_g = g_0 L_g/(1 + I/I_s), \tag{12}$$

where L_g is the length of the gain medium, g_0 is the gain under the weak excitation limit, and I and I_s are, respectively, the intensity and the saturated intensity inside the cavity. The loss of the system is expressed by

$$P = \alpha L_a C + p, \tag{13}$$

where $\alpha L_a C$ is the contribution of the absorbent solution, p denotes the conventional loss of the cavity without the sample, which is given by $p = -0.5 \ln(R_1 R_2)$, where R_1 and R_2 being the reflection coefficients of the two mirrors. At equilibrium, the following equation can be deduced:

$$\frac{I(C)}{I(0)} = 1 - \alpha L_a C \frac{g_0 L_g}{(g_0 L_g - p)(\alpha L_a C + p)}. \tag{14}$$

Numerical results (dashed line) plotted in Fig. 7(b) are obtained using the flowing parameters: $L_g = 400\ \mu\mathrm{m}$, $L_a = 150\ \mu\mathrm{m}$, $\alpha \approx 28\,000\ 1\,\mathrm{M}^{-1}\,\mathrm{cm}^{-1}$, $p = 0.1$, and $g_0 = 5\ \mathrm{cm}^{-1}$.

It should be mentioned that not only the absorption change but also the refractive index change or other changes in cavity characteristics such as scattering and molecule deposition on the surface of cavity mirrors can also significantly affect the laser emission properties. Therefore, laser intracavity measurements can be applied in many cases.

B. Single cell analyses

Optofluidic microcavity can be used for single cell biology studies. For example, they can be used to measure refractive index of cells, which depends on the content of cytoplasm. Since the concentration of proteins in cancer cells is more important than normal ones, the effective refractive index of cancer cells (1.50–1.58) is significantly larger than normal ones (1.35–1.38). With an optofluidic microcavity with gold coated optical fibers and a submerged cell holder, the effective refractive index and size of cells could be determined based on differential method, which measured the spectral shift in response to the buffer changes and the cell presence/absence.[66] Liang *et al.* replaced the fiber based cavity by a monolithic chip, which integrated microlens set for light

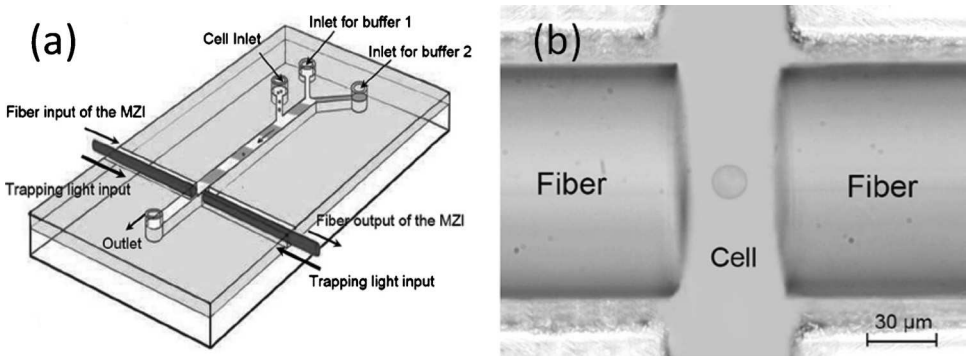

FIG. 8. (a) Schematic diagram of a buffer-modulated optofluidic device for the operation of fiber-optical trap and interferometer based measurement and (b) micrograph of a trapped cell in the center of an optofluidic microcavity (Ref. 69).

focusing, microfluidic channels for hydrodynamic focusing of cells in to a narrow stream and patterned electrodes for electrokinetic flow control. A laser diode and a mirror with actuator could also be inserted for spectral recording and it showed a high accuracy (0.25%) in the determination of effective refractive index of single living cells.[67] Alternatively, cells can be immobilized with a laser trapping force and the spectral analyses can be performed with an optofluidic microcavity formed with a pair of fiber Bragg gratings[68] or a fiber Mach–Zehnder interferometer[69] (Fig. 8). More recently, the same group has achieved a high finesse optofluidic microcavity with gold coated PDMS sidewalls and integrated liquid lenses for real time tuning using three laminar flows.[70] The results showed a detection sensitivity of 960 nm/RIU for a detection range of 0.043 RIU.

Gourley *et al.* proposed a vertical cavity surface emitting laser, which was integrated into a microfluidic device.[71] When a cell is placed inside the laser cavity, it does not only modulate the refractive index of the cavity but also perturbs the transverse confinement of the laser beam. Such a "biocavity laser" could be used for example in analyzing different blood cells. Shao *et al.* reported an integration of electrically pumped vertical cavity surface emitting laser for fluidic cavity biosensors. They also showed a dependence of laser threshold on fluid refractive index.[72] Finally, Galas[32] and Lei[33] attempted a dye laser based cytometry with integrated fiber cavities. The fabricated devices could effectively be used for high accuracy counting of cell numbers as well as identification of two types of cells with different sizes. More systematic studies have to be developed for more precise determination of the cell type, cell phase, and other specifications. When cells are grown on nanophotonic structures, they should change the optical properties of the system. Christiansen *et al.* demonstrated such a cell detection device by using polymer photonic crystal dye lasers and measuring the induced optofluidic tuning via the evanescent field of the laser.[73]

C. Single molecule detection

Based on engineered microcavities, two different approaches can be considered to achieve single molecule detection. The first one replies on the use of microtoroidal cavities of ultrahigh Q factors (Fig. 9). With a tapered optical fiber evanescently coupled to the cavity, the cavity resonance can be determined by measuring the transmission through the fiber. For refractive index monitoring, the Q factor of the microcavity increases with the increase of refractive index contrast between the cavity and its surrounding medium. This means that the measurement in water in general has lower performance than in air. Armani *et al.* measured transmission spectra by using silica cavities of different diameters (50–250 μm) in both H_2O and D_2O, showing a clear dependence of Q factor on both cavity diameter and operation wavelength.[74] For molecule detection, the cavity is surface functionalized and then immersed in a fluid containing the molecule of interest. Therefore, the interaction or attachment of the targeting molecules on the cavity surface

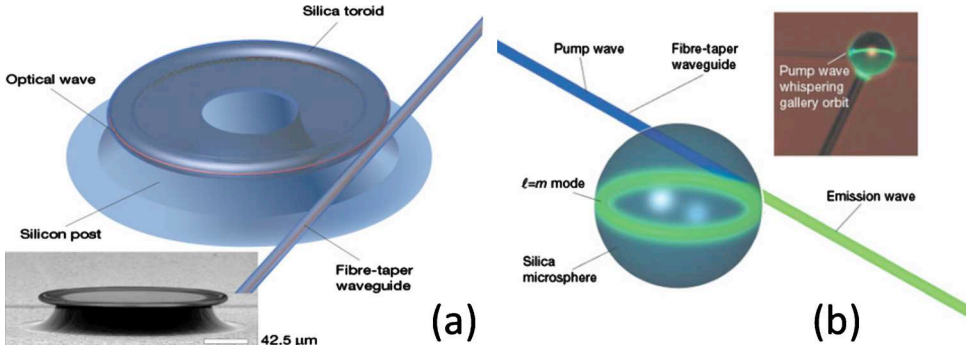

FIG. 9. Schematic of microtoroidal (a) and microspheric (b) cavities with evanescently coupled waveguides made of tapered fibers. When immersed in a solution containing molecules to be studied, the interaction of the cavity mode and the molecules bound to the edge of the cavity allows monitoring at a single molecule level (Ref. 2).

can be monitored by observation of the possible shift in the cavity resonance. For a successful monitoring, the Q-factor has to be sufficiently large so that a trapped photon can travel inside the cavity for a long time before escaped. A long time traveling also means a big chance to interact with molecules attached on the edge of the cavity. For high sensitivity monitoring, the polarizability of attached molecules should have an effect on the optical path length of the system. Armani *et al.* recently demonstrated very sensitive detection of interleukin-2 antigen from serum by using a silica microtoroid of Q factor as high as 10^8 and new thermal-optic effect.[75]

Another approach is to use highly confined light spot, which strongly interacts with localized molecules. By using advanced nanofabrication techniques, functional nanocavities can be obtained for such purposes. For example, photonic crystals with a designed trapping site could be obtained in a silicon-on-insulator wafer.[76] When a solution of colloidal quantum dots was infiltrated into the site, the measured photoluminescence spectrum of quantum dots became significantly different from the noninfiltrated ones, showing the feasibility of highly localized light-matter interaction (Fig. 10).

Integration of patterned nanophotonic structures into microfluidic devices offers many new possibilities in optofluidic studies. Erickson *et al.* fabricated nanophotonic structures in a silicon-on-insulator waveguide. Then, it was covered by fluidic channels obtained by soft-lithography. Transmission spectra could be recorded with different solutions flowed in the channel.[77] Accurate manipulation of electromagnetic waves can now also be done based on surface plasmon design and structure fabrication. Similar to the observation using dielectric photonic crystals, periodically patterned tiny holes in a metallic thin film can have a sharp wavelength selection for much enhanced light transmission.[78] Alternatively, patterned lines or circles can be used for ultrahigh resolution light localization.[79] Interaction of surface plasmonic nanostructures into optofluidic microcavities will certainly lead to new applications in chemistry and biology.

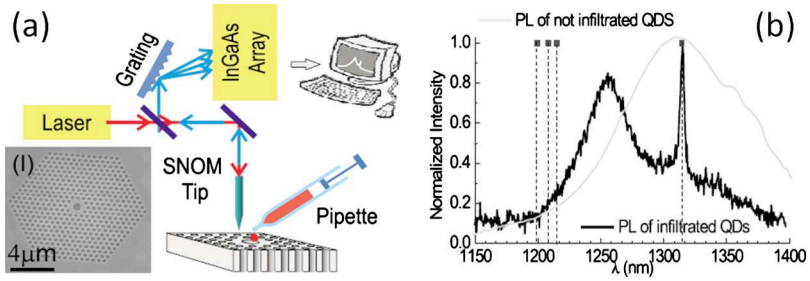

FIG. 10. (a) Schematic of a scanning near-field optical microscope for the characterization of a photonic crystal based nanocavity (i) and (b) photoluminescence spectrum of quantum dots infiltrated inside (solid line) and outside (gray line) the structure. The vertical dotted lines are calculated cavity modes (Ref. 76).

V. CONCLUSION

Most optical functionalities can be realized using the platform of microfluidics and many of them can be based on the use of optofluidic microcavities. We have attempted to review some of the current topics in this field. The starting point was a theoretical introduction of microcavity optics and microflow physics. In addition to the pressure and electro-osmotic control of microflow motions, other methods can also be used for the dynamical regulation of microflows as well as their optical properties. By reviewing different forms of microfluidic dye lasers, more developments and applications can be expected. In this regard, only few types of dye molecules (Rhodamine 6R mostly) could be tested with a quite limited spectral range. Dye molecules of different types commonly used in conventional dye lasers are able to cover a much enlarged spectral range, which have to be explored using microfluidic devices. Nonlinear optical crystals can also be integrated in optofluidic cavities, which should be useful for achieving other wavelengths in UV or IR regions.

The application field of optofluidic microcavities is broad, and the current focuses are mostly on the high sensitivity chemical and biosensing. Three examples—(i) absorption determination of small volume and low concentration solutions, (ii) characterization of single cells and, (iii) detection of single molecules—were discussed in this review to illustrate the high potential of the methods. Indeed, optofluidic microcavities can be powerful for diagnosis because of the tunable resonant interaction. For example, optofluidic cavities can be used for high sensitivity gas detection in IR wavelength windows. Of particular interests are the implementation of dye laser intracavity absorption spectroscopy and the integration of laser pumping sources and photo-detection arrays. Finally, optofluidic microcavities can be used as a part of more complex devices or systems and we conclude this review by expecting more imaginative contributions to this field.

[1] W. Koechner, *Solid-State Laser Engineering* (Springer-Verlag, New York, 1992).
[2] K. J. Vahala, Nature (London) **424**, 839 (2003).
[3] T. M. Squires and S. R. Quake, Rev. Mod. Phys. **77**, 977 (2005).
[4] A. Buguin, Y. Chen, and P. Silberzan, in *Nanoscience and Nanotechnology*, edited by M. Lahmani, P. Boisseau, and P. Houdy (Springer, Paris, 2009), Vol. 3.
[5] Y. Chen and A. Pepin, Electrophoresis **22**, 187 (2001).
[6] *Dye Laser Principles*, edited by F. J. Duarte (Academic, New York, 1990).
[7] M. A. Unger, H. P. Chou, T. Thorsen, A. Scherer, and S. R. Quake, Science **288**, 113 (2000).
[8] J. C. Galas, C. Peroz, Q. Kou, and Y. Chen, Appl. Phys. Lett. **89**, 224101 (2006); Nat. Phys. **3**, 173 (2007); Nature Photon. **1**, 78 (2007).
[9] B. Helbo, A. Kristensen, and E. Menon, J. Micromech. Microeng. **13**, 307 (2003).
[10] Y. N. Xia and G. M. Whitesides, Annu. Rev. Mater. Sci. **28**, 153 (1998).
[11] G. Escalier, "Etude de différentes structures optiques passives et actives utilisant et servant la microfluidique," Rapport de Stage Technicien en Optique, Université Paris Sud, Pairs (2002).
[12] I. Yesilyurt, "Conception, réalisation et étude de dispositifs opto-microfluidiques," Rapport de Stage DESS, Université Pierre et Marie Curie, Paris (2003).
[13] Q. Kou, I. Yesilyurt, V. Studer, M. Belotti, E. Cambril, and Y. Chen, Proceedings of the Int. Conf. MNE 2003, Cambridge; Microelectron. Eng. **73–74**, 876 (2004).
[14] D. B. Wolfe, R. S. Conroy, P. Garstecki, B. T. Mayers, M. A. Fischbach, K. E. Paul, M. Prentiss, and G. M. Whitesides, Proc. Natl. Acad. Sci. U.S.A. **101**, 12434 (2004).
[15] DARPA Center for Optofluidic Integration, http://www.biophot.caltech.edu/optofluidics/.
[16] D. Psaltis, R. S. Quake, and C. Yang, Nature (London) **442**, 381 (2006).
[17] C. Monat, P. Domachuk, and B. J. Eggleton, Nat. Photonics **1**, 106 (2007).
[18] *Optofluidics: Fundamentals—Devices and Applications*, edited by Y. Fainman, K. P. Lee, D. Psaltis, and C. Yang (McGraw-Hill, New York, 2010).
[19] Z. Li and D. Psaltis, Microfluid. Nanofluid. **4**, 145 (2008).
[20] S. A. Furman and A. V. Tikhonravov, *Basics of Optics of Multilayer Systems*, (Frontieres, Gif-sur-Yvette, 1992).
[21] J. D. Joannopoulos, S. G. Johnson, J. N. Winn, and R. D. Meade, *Photonic Crystals: Molding the Flow of Light*, 2nd ed. (Princeton University Press, Princeton, NJ, 2008).
[22] D. G. Rabus, *Integrated Ring Resonators—The Compendium* (Springer, Berlin, 2007).
[23] A. Yariv, *Quantum Electronics* (Wiley, New York, 1989).
[24] *Cavity Quantum Electrodynamics*, edited by P. R. Berman (Academic, New York, 1993).
[25] S. Haroche, Phys. Scr., T **76**, 159 (1998).
[26] C. Weisbuch, M. Nishioka, A. Ishikawa, and Y. Arakawa, Phys. Rev. Lett. **69**, 3314 (1992).
[27] Y. Chen, A. Tredicucci, and F. Bassani, Phys. Rev. B **52**, 1800 (1995).
[28] Y. Chen, F. Bassani, J. Massies, C. Deparis, and G. Neu, Europhys. Lett. **14**, 483 (1991).
[29] Q. Kou, I. Yesilyurt, G. Escalier, J. C. Galas, L. Coureau, and Y. Chen, Proc. SPIE **5641**, 112 (2005).
[30] Q. L. Kou, I. Yesilyurt, and Y. Chen, Appl. Phys. Lett. **88**, 091101 (2006).

[31] L. Lei, Y. L. Zhou, and Y. Chen, Microelectron. Eng. **86**, 1358 (2009).
[32] J. G. Calas, "Réalisation de lasers microfluidiques à colorant et application à la détection intracavité," Ph.D. thesis, University of Paris-Sud, Paris (2006).
[33] L. Lei, "Optofluidique: Dispositifs intégrés et applications en physique, chimie, et biologie, Ph.D. thesis, Université Pierre et Marie Cuire, Paris (2009).
[34] D. V. Vezenov, B. T. Mayers, R. S. Conroy, G. M. Whitesides, P. T. Snee, Y. Chan, D. G. Nocera, and M. G. Bawendi, J. Am. Chem. Soc. **127**, 8952 (2005).
[35] S. Balslev and A. Kristensen, Opt. Express **13**, 344 (2005).
[36] Z. Y. Li, Z. Y. Zhang, T. Emery, A. Scherer, and D. Psaltis, Opt. Express **14**, 696 (2006).
[37] Z. Y. Li and D. Psaltis, IEEE J. Sel. Top. Quantum Electron. **13**, 185 (2007).
[38] C. Peroz, J. C. Galas, L. Le Gratiet, Y. Chen, and J. Shi, Appl. Phys. Lett. **89**, 243109 (2006).
[39] C. Vannahme, M. B. Christiansen, T. Mappes, and A. Kristensen, Opt. Express **18**, 9280 (2010).
[40] C. Vannahme, S. Klinkhammer, A. Kolew, P.-J. Jakobs, M. Guttmann, S. Dehm, U. Lemmer, and T. Mappes, Microelectron. Eng. **87**, 693 (2010).
[41] M. Gersborg-Hansen and A. Kristensen, Appl. Phys. Lett. **89**, 103518 (2006).
[42] W. Z. Song, A. E. Vasdekis, Z. Y. Li, and D. Psaltis, Appl. Phys. Lett. **94**, 161110 (2009).
[43] E. Roy, Y. Kanamori, M. Belotti, and Y. Chen, Microelectron. Eng. **78–79**, 689 (2005).
[44] M. Belotti, K. Torres, E. Roy, and Y. Chen, J. Appl. Phys. **99**, 024309 (2006).
[45] M. Belotti, K. Torres, E. Roy, A. Pepin, D. Gerace, L. C. Andreani, M. Galli, and Y. Chen, Microelectron. Eng. **83**, 1773 (2006).
[46] J. Shi, A. P. Fang, L. Malaquin, and Y. Chen, Appl. Phys. Lett. **91**, 153114 (2007).
[47] J. Shi, X. F. Ni, and Y. Chen, Langmuir **23**, 11377 (2007).
[48] J. Hu, J. Shi, F. Zhang, and Y. Chen, Microelectron. Eng. **87**, 726 (2010).
[49] A. Pépin, P. Youinou, V. Studer, and Y. Chen, Microelectron. Eng. **61–62**, 927 (2002).
[50] V. Studer, A. Pepin, and Y. Chen, Appl. Phys. Lett. **80**, 3614 (2002).
[51] L. Lei, I. L. Mattos, and Y. Chen, Microelectron. Eng. **85**, 1318 (2008).
[52] L. Lei, H. Li, J. Shi, and Y. Chen, Rev. Sci. Instrum. **81**, 023103 (2010).
[53] J. Orfanidis, *Electromagnetic Waves and Antennas* (ECE, Rutgers University, Piscataway, 2004), Chap. 5, available online only, http://www.ece.rutgers.edu/orfanidi/ewa/.
[54] J. C. Galas, J. Torres, M. Belotti, Q. Kou, and Y. Chen, Appl. Phys. Lett. **86**, 264101 (2005).
[55] Z. Y. Li, Z. Zhang, A. Scherer, and D. Psaltis, Proceedings of the IEEE LEOS Summer Topics, Portland, 2007.
[56] J. D. Suter, Y. Sun, D. J. Howard, J. Viator, and X. Fan, Opt. Express **16**, 10248 (2008).
[57] Y. Z. Sun, J. D. Suter, and X. D. Fan, Opt. Lett. **34**, 1042 (2009).
[58] W. Z. Song and D. Psaltis, Appl. Phys. Lett. **96**, 081101 (2010).
[59] Z. Li, Z. Zhang, A. Scherer, and D. Psaltis, Opt. Express **14**, 10494 (2006).
[60] S. K. Y. Tang, Z. Y. Li, A. R. Abate, J. J. Agresti, D. A. Weitz, D. Psaltis, and G. M. Whitesides, Lab Chip **9**, 2767 (2009).
[61] G. M. Whitesides, Nature (London) **442**, 368 (2006).
[62] D. Janasek, J. Franzke, and A. Manz, Nature (London) **442**, 374 (2006).
[63] H. Craighead, Nature (London) **442**, 387 (2006).
[64] A. J. deMello, Nature (London) **442**, 394 (2006).
[65] J. El-Ali, P. K. Sorger, and K. F. Jensen, Nature (London) **442**, 403 (2006).
[66] W. Z. Song, X. M. Zhang, A. Q. Liu, C. S. Lim, P. H. Yap, and H. M. M. Hosseini, Appl. Phys. Lett. **89**, 203901 (2006).
[67] X. J. Liang, A. Q. Liu, C. S. Lim, T. C. Ayi, and P. H. Yap, Sens. Actuators, A **133**, 349 (2007).
[68] L. K. Chin, A. Q. Liu, X. M. Zhang, C. S. Lim, J. H. Ng, J. Z. Hao, and S. Takahashi, Appl. Phys. Lett. **91**, 243901 (2007).
[69] W. Z. Song, A. Q. Liu, S. Swaminathan, C. S. Lim, P. H. Yap, and T. C. Ayi, Appl. Phys. Lett. **91**, 223902 (2007).
[70] L. K. Chin, A. Q. Liu, C. S. Lim, C. L. Lin, T. C. Ayi, and P. H. Yap, Biomicrofluidics **4**, 024107 (2010).
[71] P. L. Gourley, J. Phys. D: Appl. Phys. **36**, R228 (2003).
[72] H. Shao, D. Kumar, and K. L. Lear, IEEE Sens. J. **6**, 1543 (2006).
[73] M. B. Christiansen, J. M. Lopacinska, M. H. Jakobsen, N. A. Mortensen, M. Dufva, and A. Kristensen, Opt. Express **17**, 2722 (2009).
[74] D. K. Armani, B. Min, and K. J. Vahala, Appl. Phys. Lett. **87**, 151118 (2005).
[75] A. M. Armani, R. P. Kulkarni, S. Fraser, R. C. Flagan, and K. J. Vahala, Science **317**, 783 (2007).
[76] S. Vignolini, F. Riboli, F. Intonti, M. Belotti, M. Gurioli, Y. Chen, M. Colocci, L. C. Andreani, and D. S. Wiersma, Phys. Rev. E **78**, 045603 (2008).
[77] E. D. Erickson, T. Rockwood, T. Emery, A. Scherer, and D. Psaltis, Opt. Lett. **31**, 59 (2006).
[78] T. W. Ebbesen, H. J. Lezec, H. F. Ghaemi, T. Thio, and P. A. Wolff, Nature (London) **391**, 667 (1998).
[79] C. Genet and T. W. Ebbesen, Nature (London) **445**, 39 (2007).